Applied Surface Science 456 (2018) 602–608

Contents lists available at ScienceDirect

Applied Surface Science

journal homepage: www.elsevier.com/locate/apsusc

Full Length Article

Excellent oil-water separation under external pressure: Controllable critical pressure and separation efficiency by well-designed hierarchical mesh structure

Xinguo Qiu[a], Zhe Yang[a], Huaping Wu[a,b,*], Jing Guo[a], Zheng Zhang[a], Jie Feng[c], Guozhong Chai[a], Aiping Liu[d,e,*]

[a] Key Laboratory of E&M (Zhejiang University of Technology), Ministry of Education & Zhejiang Province, Hangzhou 310014, China
[b] State Key Laboratory for Strength and Vibration of Mechanical Structures, Xi'an Jiaotong University, Xi'an 710049, China
[c] College of Materials Science & Engineering, Zhejiang University of Technology, Hangzhou 310014, China
[d] Center for Optoelectronics Materials and Devices, Zhejiang Sci-Tech University, Hangzhou 310018, China
[e] State Key Laboratory of Structural Analysis for Industrial Equipment, Dalian University of Technology, Dalian 116024, China

ARTICLE INFO

Keywords:
Oil-water separation
Critical pressure
External pressure
Separation efficiency
Hierarchical mesh structure

ABSTRACT

With the increase of oily wastewater, the improvement of separation efficiency for oil-water emulsion under external pressure is an urgent task to resolve. As an important indicator for the separation result, the separation efficiency is affected by the wetting transition and external pressure. In this contribution, we built a model of hierarchical mesh structure and analyzed the effect of the space of mesh microstructure and the solid fraction of mesh nanostructure on energy barrier and critical pressure, which was further confirmed by experiment. The influences of external pressure on separation efficiency were also investigated experimentally, verifying the reasonability of critical pressure. This work provides guidance for designing and choosing the mesh structure applied in the separation of oil-water mixture under external pressure to get an excellent process efficiency and separation efficiency.

1. Introduction

Because of the increasing water pollution induced by the oil spills and chemical leakage, oil-water separation with high separation efficiency is given great attention. Conventional separation techniques, such as gravity separation, flotation and skimming flotation can separate the free oil-water mixtures. However, they are not applicable for the oil-water emulsions [1] due to the small size of droplets. Superwetting materials as candidates for oil-water separation have been given great attention for their potential application on fundamental research and industrial production [2–4]. Since a stainless steel mesh coated with a Teflon film is firstly reported the potential for oil-water separation [5], a number of superwetting materials [6–11] and their modified porous structures [5,12–16] are developed to form various micro/nanostructure for effective oil-water emulsion separation. The microstructures of these materials play an important role in the oil absorption [17] and water repellent [18,19]. Meanwhile, the nanostructures can improve the structure wettability [20–22] and enhance the ability of resisting wetting transition [23–25] and oil absorption [26,27]. Taking advantage of these properties, the separation efficiency can be improved by using the superwetting materials with well-designed micro/nanostructure.

In general, the excellent separation in experiments is driven by gravity and done in quasi static [28,29]. The membranes need endure various impact forces when the mixture fluxes to the membranes in practical process. Furthermore, an external pressure is usually applied to the membranes to improve the oil flux and enhance the process efficiency [30,31]. In this case, the impact force and external pressure have the risk of exceeding water critical pressure [32] (the surface tension of water hinders the movement of three phase contact line), and the water is forced to penetrate trough the membranes, decreasing the separation efficiency quickly. Therefore, the critical pressure is an important parameter for oil-water separation. A lot of groups have tested the maximum pressure that the membrane can endure [33–38]. For example, Jiang et al. [33] took advantage of the superhydrophilic and underwater superoleophobic hydrogel coatings on porous metal substrates and gave the average intrusion pressures for all the oil above 1.0 kPa. Jin et al. [34] used phase-inversion process to get porous poly

* Corresponding authors at: Key Laboratory of E&M (Zhejiang University of Technology), Ministry of Education & Zhejiang Province, Hangzhou 310014, China (H. Wu). Center for Optoelectronics Materials and Devices, Zhejiang Sci-Tech University, Hangzhou 310018, China (A. Liu).
E-mail addresses: wuhuaping@gmail.com (H. Wu), liuaiping1979@gmail.com (A. Liu).

https://doi.org/10.1016/j.apsusc.2018.06.178
Received 1 February 2018; Received in revised form 16 June 2018; Accepted 19 June 2018
Available online 20 June 2018
0169-4332/

(vinylidene fluoride) (PVDF) membranes with the separation efficiency as high as 99.95% at gravity driving and the endurable pressure of the membranes reached to 17 kPa. Tuteja et al. [35,36] and Chen et al. [30] applied gravity and external pressure to oil-water emulsions in the experiment. However, the explicit relationship between the external pressure and the separation efficiency was seldom involved, especially when external pressure gradually broke through the critical pressure. Since the droplet wettability and the critical pressure are all related to the network structure, a well-designed mesh structure is helpful for the improvement of separation efficiency under external pressure.

In this work, we designed a hierarchically structured mesh and investigated the relation of structure parameter of mesh and critical pressure by building a droplet model dipped on a microstructured mesh with nanoparticles modified on its surface. The impact of microstructure size and solid fraction of nanoparticle on energy barrier and critical pressure was analyzed, which was further proved by designing a precise experiment. Finally, the relationship of external pressure and separation efficiency of oil-water emulsion was established by experimentally, verifying the reasonability of critical pressure. This can offer some suggestions in dealing with the oily wastewater in order to achieve excellent process efficiency and separation efficiency.

2. Experimental

2.1. Preparation of hydrophobic TiO_2 coating

A mixture of 0.10 g TiO_2 particles (25 nm in diameter, Aladdin Inc.) and 10 mL alcohol was ultrasonically treated for 30 min to get well-distributed suspension solution. Then 0.20 mL Trimethoxy (octadecyl) silane (TMOS) was added into the suspension mixture for 12-h reaction at room temperature to obtain a hydrophobic TiO_2 particle suspension [39].

2.2. Modification of copper mesh

Commercial copper meshes (Jiuji Wire Mesh Products Co. Ltd) with four different sizes (microstructure space of 0.090, 0.10, 0.13 and 0.16 mm) were put into a hydrogen nitrate solution (10 V/V%) to remove the oxide on their surfaces. Then the copper meshes were ultrasonically washed by acetone, alcohol and water for 10 min, respectively, and dried in stove. After the copper mesh was sheared into a circle with the diameter of 30 mm, it was immersed in the hydrophobic TiO_2 suspension solution for 2 min. Five samples were obtained by repeating the modification process for 2, 6, 10, 14 and 18 times, respectively. All samples were dried in a 100 °C oven for one hour.

2.3. Characterization of copper meshes

The morphology and structure of copper meshes before and after modification with TiO_2 were investigated by a field emission scanning electron microscope (FESEM, Hitachi S4800), X-ray diffractometer (XRD, Bruker AXS D8) and Raman spectrometer (Thermo Fisher DXR with a He-Ne laser, λ = 632.8 nm). The contact angle measurement was performed by using a contact angle goniometer (OCA20, GER) at room temperature.

2.4. Measurement of the critical pressure

Before we did the experiment, we cut the square copper mesh into a circle that is in line with the inner diameter of the Teflon pipe (A). Then the copper mesh was placed on the edge of the Teflon pipe (B) with thread on its sidewall (Fig. 1a). Another Teflon pipe (A) with thread on its sidewall could engage with the Teflon tube (B) and sealed at the top of the thread of the Teflon tube (A) by a rubber washer (Fig. 1b). Put the sealed connecting tube into the water, and apply a pressure to the other end of the Teflon tube A. No air bubbles are generated at the seal, indicating that the measurement system has good tightness. Then this joint pipe was clamped on iron support stand and a clean beaker was put under the pipe (Fig. 1c) before putting them into a vacuum drying oven (Fig. 1d). Close the oven and open the vacuuming button. When the droplets dripped from the pipe, the number on the meter of the oven was the value of the critical pressure ΔP_{max}.

3. Result and discussion

3.1. Energy analysis

3.1.1. Energy barrier

The influence of micro/nanoscale structure on wetting states and wetting transition was analyzed in our previous works [20,23]. For a droplet dipped on a mesh surface with micro/nanostructure (Fig. 2a), the equation of apparent contact angle (θ) of the droplet is derived (see Part S1 in supporting information). From Fig. S1, we can propose that the θcan be improved by decreasing the areal fraction of the solid-liquid interface on the nanostructure of modified mesh (f_2) or increasing the space of microstructure (l) (Fig. 2b). When some external disturbance, such as vibration [40], impact [41], evaporation [42], are imposed on the droplet, the wetting state of the droplet will change, penetrating the mesh microstructure. In the practical process of oil-water separation, the oil-water mixture does not simply drop on the mesh surface with micro/nanostructures slowly. There is a process of dumping when the separation is being done. Therefore, it is very meaningful to analyze the energy barrier ΔG which is needed to be overcome when the micro/nanostructure of mesh is being penetrated.

Here we build a model to analyze the change of ΔG specifically (Fig. 2b). The ΔG that the droplet needs to overcome consists of two parts when the droplet penetrates the micro/nanostructure of mesh. For the first one, when the included angle between meniscus tangent and micro/nanostructure surface approaches to the advanced contact angle (θ_{adv}), the area of liquid-air interface will increase and the three phase contact line will move down. In this case, the energy barrier of this part is the increment of

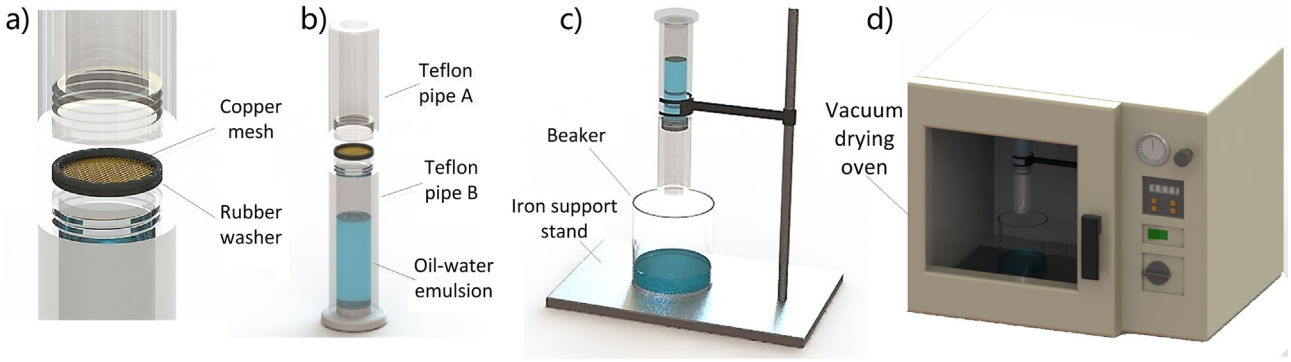

Fig. 1. (a) Local enlarged view and (b) panorama of threaded seal connection for the oil-water separation device. (c) Configuration of oil-water separation device for critical pressure measurement. (d) Measurement of critical pressure in the vacuum drying oven.

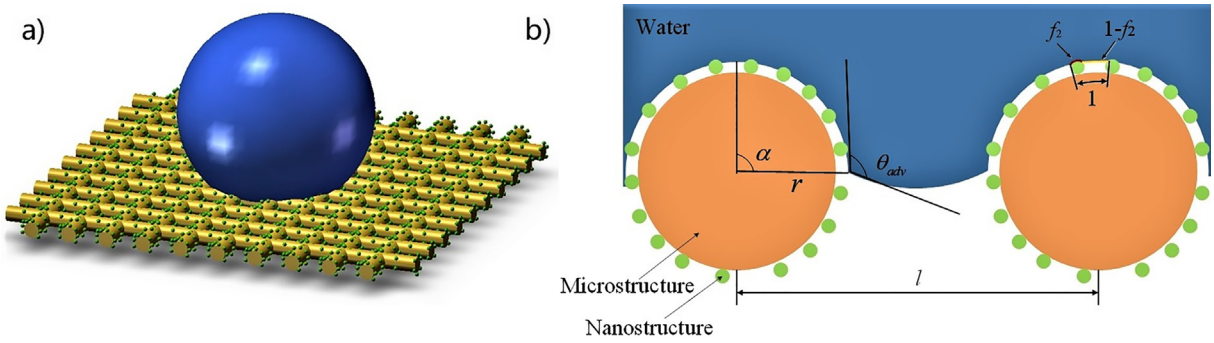

Fig. 2. (a) 3D diagram of a droplet dipped on a mesh surface with micro/nanostructure. (b) Schematic diagram of the liquid wetting of the microstructure surface of mesh with nanoparticles on it.

the liquid-vapor interface area. The second one is the energy that the three phase contact line moves from the top side to the down side. The sum of the two parts is

$$\Delta G = \frac{S}{l^2}(-\gamma_{LV} \times 4l \times \alpha r \times \cos\theta_{adv} + \gamma_{LV} \times \Delta A) \tag{1}$$

with $\Delta A = l^2\left(\frac{\pi}{2}\frac{1}{1+\sin\theta} - 1\right)$. Here S is the area of mesh structure, r is the radius of microstructure, γ_{LV} is the surface tensions of liquid-vapor interface, and $\alpha$is the included angle of the three phase contact line and the vertical center line of the mesh microstructure.

Furthermore, θ_{adv} can be expressed by a Cassie-Baxter (CB) equation [43]:

$$\cos\theta_{adv} = f_2 \cos\theta_{adv0} + f_2 - 1 \tag{2}$$

in which $\theta_{adv0}$is the intrinsic advanced contact angle on smooth surface. Then we introduce a nondimensionalized energy barrier $\Delta G^*(\Delta G^* = \frac{\Delta G}{\gamma_{LV} S})$, which can be expressed as

$$\Delta G^* = -4 \times \alpha\frac{r}{l} \times \cos\theta_{adv} + \frac{\pi}{2}\frac{1}{1+\sin\theta_{adv}} - 1. \tag{3}$$

3.1.2. Energy barrier analysis

In the process of three phase contact line moving down, ΔG^* can be influenced by the morphology size (l, r, f_2) and θ_{adv0}. When l/r keeps constant, as shown in Fig. 3(a), with the increase of θ_{adv0}, smaller f_2 presents less influence on ΔG^*. This is related to the decreased influence of f_2 on θ_{adv} with θ_{adv0} increasing. Meanwhile, the ΔG^*decreases with the increase of the microstructure characteristic length l/r at a given f_2 andθ_{adv0} (Fig. 3b), but the θ increases in the same case (Fig. S1). This can be explained that the area of the copper mesh is fixed, the pitch l becomes larger, and the area where the droplet needs to infiltrate becomes smaller. Meanwhile, according to Eqs. (2) and (3), the larger the micro-structure spacing l is, the smaller the required energy barrier ΔG^* is. This means that an excellent superhydrophobic substrate is necessary in the experiment of oil-water separation. Consider the established l/r for a given mesh structure, we would improve the hydrophobicity of substrate.

3.2. Critical pressure analysis

3.2.1. Critical pressure

When the meniscus penetrates through the microstructure, the movement of the three phase contact line is blocked by the liquid surface tension. Therefore, a pressure ΔP [44,45] needs to be overcome with the formulation of

$$\Delta P = \frac{-\gamma_{LV}\cos\theta_{adv} \times 4}{l - 2 \times r\sin\alpha}. \tag{4}$$

Eq. (4) is deduced by considering the cross sectional area A of the hole (the difference between a rectangular area and two semicircular areas), which is

$$A = \left(\frac{l}{2}\right)^2 - \frac{l}{2}r\sin\alpha. \tag{5}$$

We use the water-in-oil fluid mixtures (cyclohexane-water emulsions and trichloromethane-water emulsions) in this paper. The oil is a large environment and $\gamma_{LV}$is the surface tension of the oil-vapor interface.

3.2.2. Critical pressure prediction

In the process of meniscus going down, the pressure which is needed to be overcome is different because of the curved surface of microstructure. The meniscus can penetrate through the microstructure, only if the meniscus overcomes the critical pressure ΔP_{max}. When l, r, $\gamma_{LV}$and θ_{adv}keep constant (Fig. 4), the ΔPthat the meniscus needs to overcome reaches to the maximum value when $\alpha = 90°$.

In order to clearly analyze the effect of l, $\theta_{adv0}$and f_2 on ΔP_{max}, we consider a mesh with hierarchically structured surface. At a given $l = 0.050$ (Fig. 5a), with the increasing of θ_{adv0}, the trend of ΔP_{max}

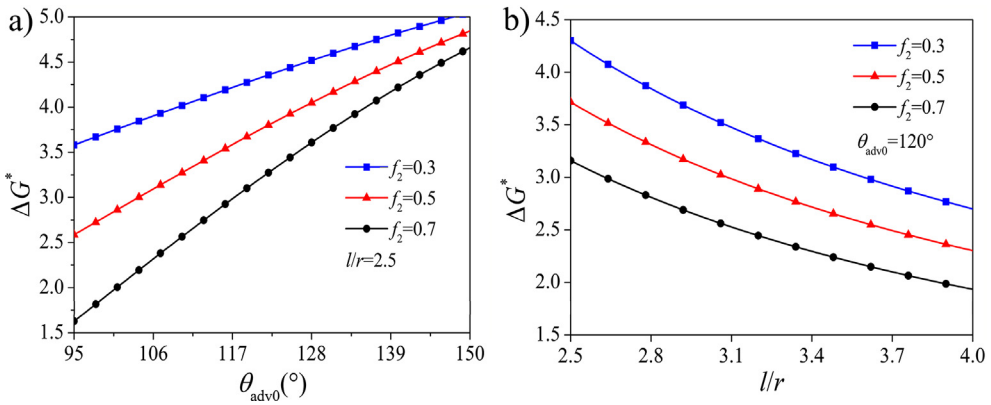

Fig. 3. (a) Relation between θ_{adv0} and the energy barrier ΔG^*, (b) relation between l/r and the energy barrier ΔG^*.

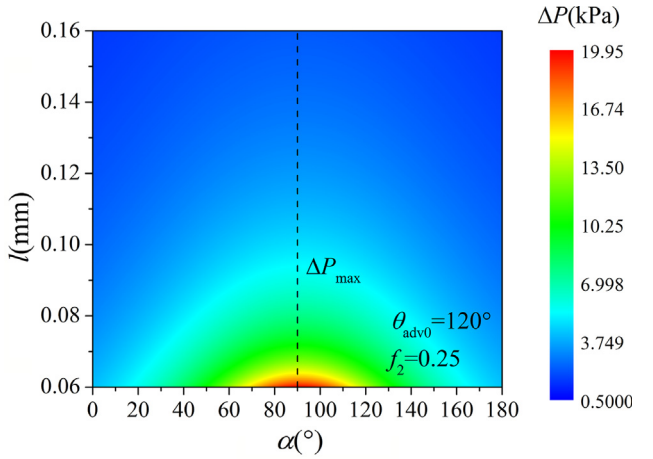

Fig. 4. Movement of three phase contact line, the critical pressure ΔP_{max} is reached at $\alpha = 90°$.

variation is similar to ΔG^*. ΔG^* indicates the energy of three-phase contact lines moving through the copper mesh. This means that ΔG^*can be adjusted through the l/r and changes approximately linearly with decreasing l/r (Fig. 3b). It can be seen from Fig. 5b that ΔP_{max} is an inverse proportional function of l, for a sufficiently small l, ΔP_{max} will increase to tens of kilopascals even hundreds of kilopascals [30,34].

Furthermore, the ΔP_{max} can be obtained by experimental measurement. First, the copper meshes with different spaces (0.090 mm, 0.10 mm, 0.13 mm and 0.15 mm) were modified by TiO_2 nanoparticles for different times. After TiO_2 modification, the surfaces of copper meshes are rougher (Fig. 6). In order to ensure the uniformity of the TiO_2 coating, we generally deal with several pieces of copper mesh simultaneously. The thickness from 10 points in different area of the sample surface presents an error about 0.5 μm, indicating the homogeneity of the coatings. The XRD patterns of copper meshes before and after TiO_2 modification prove that the TiO_2 nanoparticles are attached on the copper mesh surface (Fig. S2a). The Raman characteristic peaks related to TMOS indicate the successful modification of TMOS on the TiO_2 anchored on the mesh surface (Fig. S2b). The copper meshes which have the same modification time possess the same θ_{adv}. With the increase of modification time, the $\theta_{adv}$of five different samples (modify 2, 6, 10, 14 and 18 times) are 149.2°, 153.8°, 158.1°, 163.7° and 168.3°, respectively (Fig. 7). By experimental measurement of the ΔP_{max}, the relation between $\Delta P_{max}$and $\theta_{adv}$is displayed in Fig. 7. The experiment results agree well with the theoretical ones calculated by Eq. (4).

3.2.3. Relationship between critical pressure and separation efficiency

The TiO_2 coating modified with TMOS is not only hydrophobic, but also oleophilic [39,46]. In our experiment, the well-modified copper mesh was fastened in Teflon pipe. The oil-water emulsion with the molar concentration ratio (M_{water}:M_{oil}) of 3:7 (the volume of liquid is 30 mL) was prepared by mixing water and trichloromethane (or cyclohexane) using a stir bar (at 2000 RPM) for 30 min. The trichloromethane has larger density than water while cyclohexane has

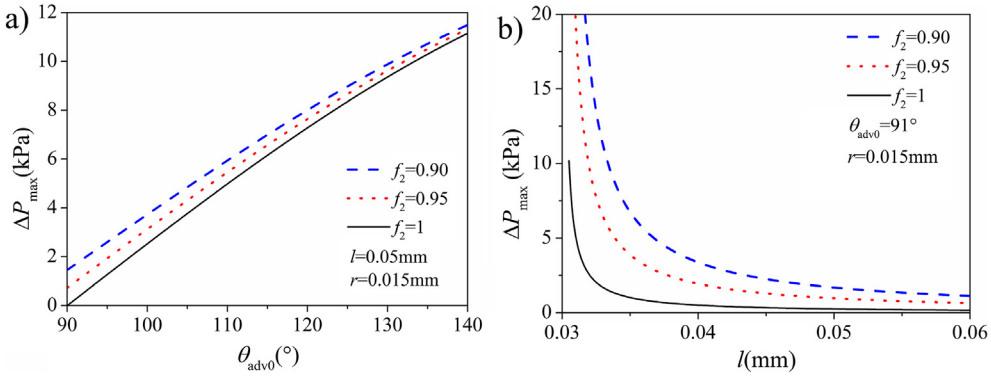

Fig. 5. (a) Effect of θ_{adv0} on the critical pressure ΔP_{max} for alterablef_2, (b) effect of l on the critical pressure ΔP_{max} for alterablef_2.

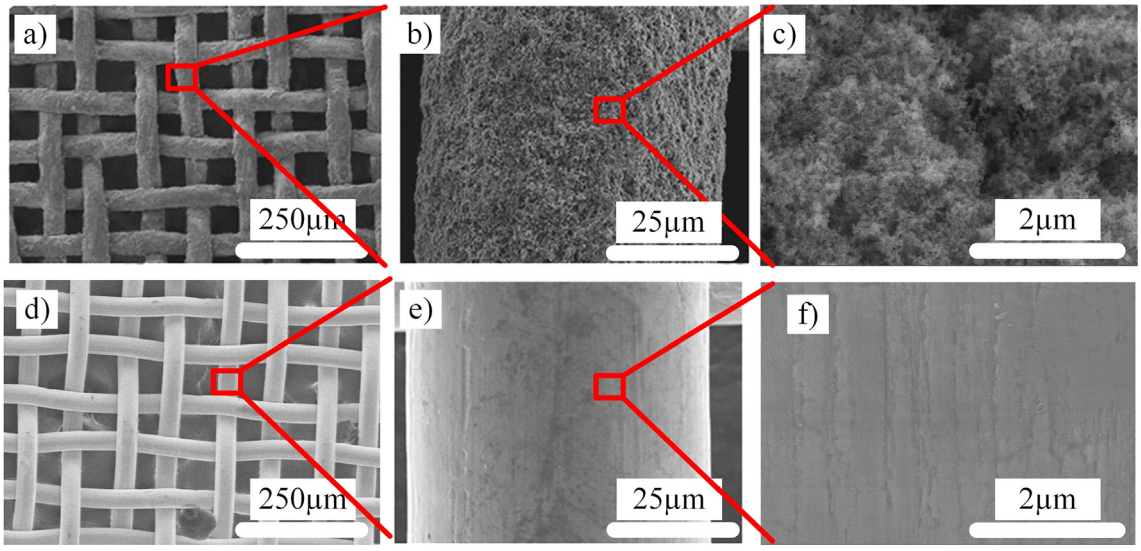

Fig. 6. SEM images of (a) copper mesh modified by TiO_2 coating (b, c are the enlarged views of one copper wire), (d) copper mesh without any processing (e, f are the enlarged views of one copper wire). The space of mesh microstructure is 0.090 mm.

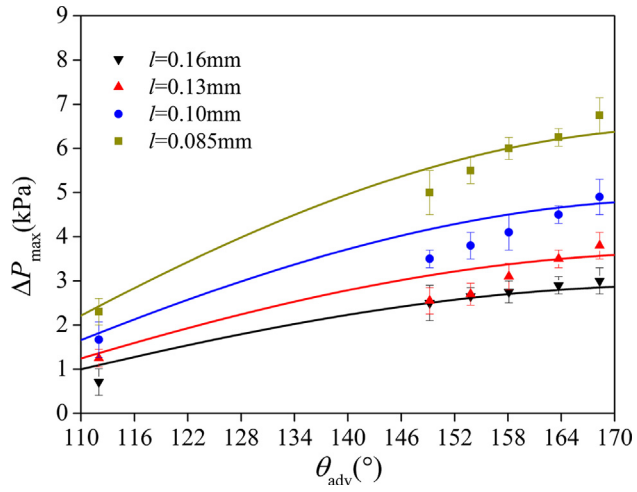

Fig. 7. Comparison between the theoretical ΔP_{max}(line) with the experiment ones (spot) with various θ_{adv} for four different copper meshes. The points from left to right correspond to the data of copper meshes modified for 0, 2, 6, 10, 14 and 18 times, respectively.

lower density than water (water is dyed by methylene blue). As presented in Fig. 8, the oil-water emulsion was separated very well, whether the oil is trichloromethane (Fig. 8a and b) or cyclohexane (Fig. 8c). Besides, the high separation efficiency (the weight ratio of retained water to original water in the oil-water emulsion [47]) about 99% at the quasi state can be obtained when treating the n-Butanol-water emulsion by using the TiO_2 modified copper mesh for 30 recycles (Fig. S3a). Changing the oil-water systems, the separation efficiency over 99% are all obtained after 30 recycles (Fig. S3b).

In order to improve the process efficiency, external pressure will be applied. In our experiment, five different external pressures are adopted

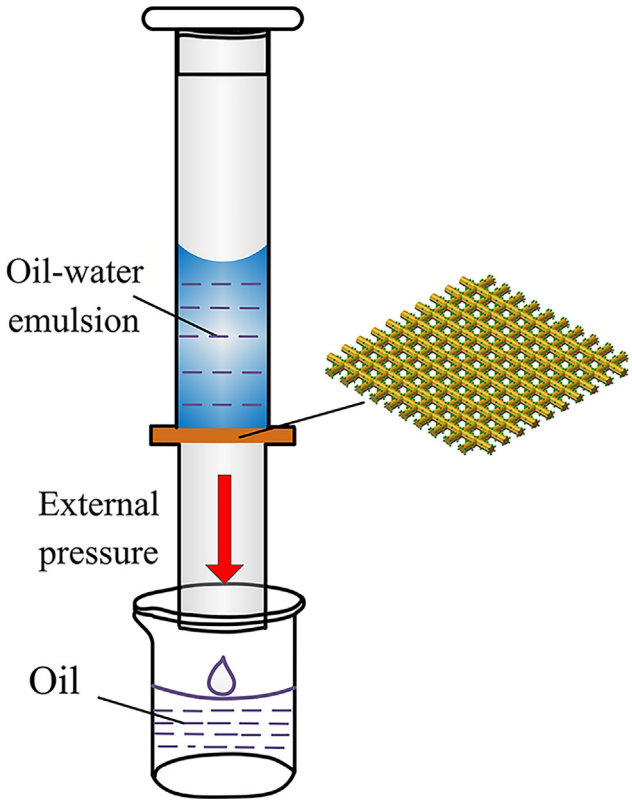

Fig. 9. Separation process of oil-water emulsion under external pressure.

for the emulsion separations (trichloromethane-water mixture). The separation experiment similar to the ΔP_{max} one is presented in Fig. 9, which finishes when the emulsion stops going down. For the copper

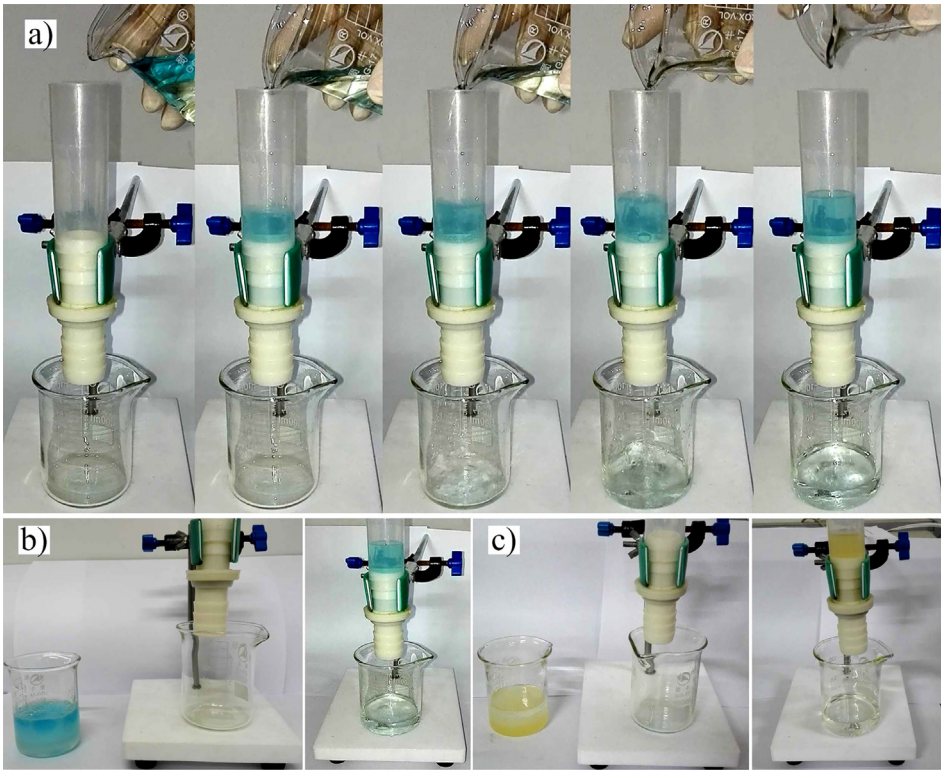

Fig. 8. Oil-water separation process by using the TiO_2 modified copper mesh (microstructure space of 0.10 mm): (a) separation process of trichloromethane-water emulsion, (b) photos of trichloromethane-water emulsion before and after separation, (c) photos of cyclohexane -water emulsion before and after separation.

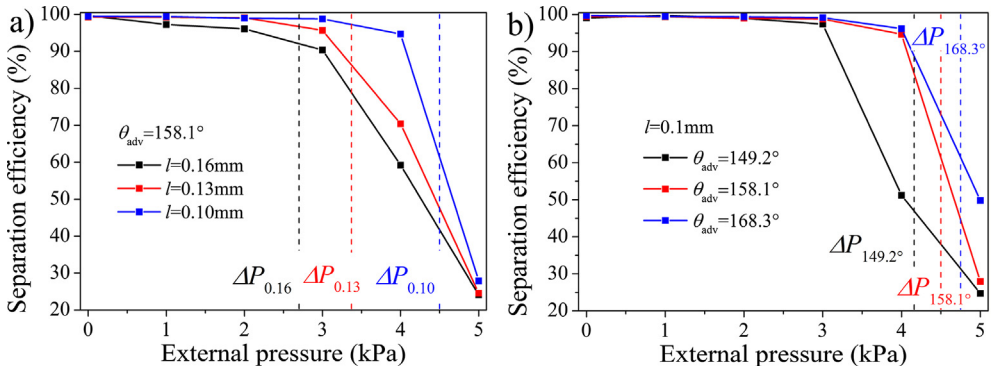

Fig. 10. Relation of separation efficiency with external pressure when using (a) different copper meshes with same modification times, (b) same copper meshes with different modification times. The dotted lines are the calculated critical pressure.

meshes with different space structures (structure space of 0.10 mm, 0.13 mm and 0.16 mm) and same modification times, we calculate the ΔP_{max} are 4.5 kPa ($\Delta P_{0.10}$), 3.37 kPa ($\Delta P_{0.13}$) and 2.7 kPa ($\Delta P_{0.16}$), respectively, by using Eq. (4). When the external pressure is applied, the separation efficiency decreases with the increase of external pressure (Fig. 10a). Specially, the separation efficiency is 94.7% by using the 0.10-mm copper mesh at a 4.0 kPa external pressure, which sharply decreases to about 28% when a 5.0 kPa external pressure is used. This indicates that an efficient critical pressure ΔP_{max} is existent. When the applied exceeds the ΔP_{max}, the copper mesh loses efficacy. Similar phenomena of obvious decreased separation efficiency are also observed in the cases of 0.13 mm and 0.16 mm copper meshes when exorbitant external pressures are employed. Analogously, the separation efficiency can be improved by controlling the modification time of copper mesh (l = 0.1 mm). The θ_{adv} of copper mesh increases from 149.2° to 168.3° when the modification time increases from 2 to18, which induces the change of ΔP_{max} from 4.16 kPa ($\Delta P_{149.2}$) to 4.75 kPa ($\Delta P_{168.3}$) (Fig. 10b). Therefore, by reasonably selecting and controlling the mesh structure and external pressure, satisfactory high separation efficiency above 94% is realizable. Additionally, the relationship of external pressure and separation efficiency by using other three mesh structures are also provided and shown in Fig. S4. Our results indicate that just by simply modifying the commercial copper mesh and controlling the mesh structure and θ_{adv}, we can obtain the ΔP_{max} to better carry out oil-water separation experiment under external pressure to get an excellent process efficiency and separation efficiency.

4. Conclusion

In this paper, the effects of the microstructure space and nanostructure solid fraction of mesh on the energy barrier and critical pressure in the separation process of oil-water emulsion are investigated by building a model of hierarchical mesh structure. The decreasing of microstructure space can increase the apparent contact angle [20,23] but reduce the energy barrier. The change trend of the critical pressure obtained from theoretically is well proved by experiment results. The relationship between separation efficiency and the external pressureis also analyzed by the separation experiments, verifying the reasonability of critical pressure. Our results indicate that just by simply modifying the commercial copper mesh and controlling the mesh structure and apparent contact angle, we can adjust the critical pressure. This can give advices to industrial oily waste water treatments to optimize experiment process under external pressure and improve separation efficiency and process efficiency.

Acknowledgments

This work was supported by the National Key Research and Development Program of China (Grant No. 2017YFB0603740), the National Natural Science Foundation of China (Grant Nos. 11672269, 51675485, 51572242), the Zhejiang Provincial Natural Science Foundation of China (Grant Nos. Q17E050031, LQ17E050007), the Zhejiang Provincial Public Welfare Technology Application Research Projects (Grant No. 2016C31041) and the Open Research Fund Program of State Key Laboratory of Structural Analysis for Industrial Equipment, Dalian University of Technology (Grant No. GZ1704).

References

[1] M. Cheryan, N. Rajagopalan, Membrane processing of oily streams. Wastewater treatment and waste reduction, J. Membr. Sci. 151 (1998) 13–28.
[2] N. Shirtcliffe, G. McHale, M. Newton, G. Chabrol, C. Perry, Dual-scale roughness produces unusually water-repellent surfaces, Adv. Mater. 16 (2004) 1929–1932.
[3] L. Zhai, F.C. Cebeci, R.E. Cohen, M.F. Rubner, Stable superhydrophobic coatings from polyelectrolyte multilayers, Nano. Lett. 4 (2004) 1349–1353.
[4] N. Wang, Y. Lu, D. Xiong, C.J. Carmalt, I.P. Parkin, Designing durable and flexible superhydrophobic coatings and its application in oil purification, J. Mater. Chem. A 10 (2016) 4107–4116.
[5] L. Feng, Z. Zhang, Z. Mai, Y. Ma, B. Liu, L. Jiang, D. Zhu, A super-hydrophobic and super-oleophilic coating mesh film for the separation of oil and water, Angew. Chem. Int. Ed. 43 (2004) 2012–2014.
[6] H. Wang, H. Zhou, W. Yang, Y. Zhao, J. Fang, T. Lin, Selective, spontaneous one-way oil-transport fabrics and their novel use for gauging liquid surface tension, ACS Appl. Mater. Interf. 7 (2015) 22874–22880.
[7] Z. Xu, Y. Zhao, H. Wang, X. Wang, T. Lin, A superamphiphobic coating with an ammonia-triggered transition to superhydrophilic and superoleophobic for oil-water separation, Angew. Chem. Int. Ed. 54 (2015) 4527–4530.
[8] M. Liu, J. Li, L. Shi, Z. Guo, Stable underwater superoleophobic conductive polymer coated meshes for high-efficiency oil–water separation, RSC Adv. 5 (2015) 33077–33082.
[9] X. Chen, J. Wu, R. Ma, M. Hua, N. Koratkar, S. Yao, Z. Wang, Nanograssed micropyramidal architectures for continuous dropwise condensation, Adv. Funct. Mater. 21 (2011) 4617–4623.
[10] S. Li, J. Liu, J. Hou, Curvature-driven bubbles or droplets on the spiral surface, Sci. Rep. 6 (2016) 37888.
[11] B. Emami, T.M. Bucher, H.V. Tafreshi, D. Pestov, M. Gad-el-Hak, G.C. Tepper, Simulation of meniscus stability in superhydrophobic granular surfaces under hydrostatic pressures, Colloid Surf. A-Physicochem. Eng. Asp. 385 (2011) 95–103.
[12] D. Zang, C. Wu, R. Zhu, W. Zhang, X. Yu, Y. Zhang, Porous copper surfaces with improved superhydrophobicity under oil and their application in oil separation and capture from water, Chem. Commun. 49 (2013) 8410–8412.
[13] X. Gao, L.-P. Xu, Z. Xue, L. Feng, J. Peng, Y. Wen, S. Wang, X. Zhang, Dual-scaled porous nitrocellulose membranes with underwater superoleophobicity for highly efficient oil/water separation, Adv. Mater. 26 (2014) 1771–1775.
[14] M. Liu, J. Li, Z. Guo, Polyaniline coated membranes for effective separation of oil-in-water emulsions, J. Colloid Interf. Sci. 467 (2016) 261–270.
[15] J. Li, C. Xu, Y. Zhang, R. Wang, F. Zha, H. She, Robust superhydrophobic attapulgite coated polyurethane sponge for efficient immiscible oil_water mixture and emulsion separation, J. Mater. Chem. A 4 (2016) 15546–15553.
[16] Z. Xue, Y. Cao, N. Liu, L. Feng, L. Jiang, Special wettable materials for oil_water separation, J. Mater. Chem. A 2 (2014) 2445–2460.
[17] J. Guo, F. Yang, Z. Yang, Fabrication of stable and durable superhydrophobic surface on copper substrates for oil–water separation and ice-over delay, J. Colloid Interf. Sci. 466 (2016) 36–43.
[18] M.M. Amrei, H.V. Tafreshi, Effects of hydrostatic pressure on wetted area of submerged superhydrophobic granular coatings. Part 1: mono-dispersed coatings, Colloids Surf. A 465 (2015) 87–98.
[19] R. Wang, S. Bai, Wettability of laser micro-circle-dimpled SiC surfaces, Appl. Surf. Sci. 346 (2015) 107–110.
[20] B. Wu, H. Wu, Z. Zhang, C. Dong, G. Chai, Thermodynamic analysis of stable

wetting states and wetting transition of micro/nanoscale structured surface, Acta Phys. Sin. 64 (2015) 176801.
[21] P. Hao, C. Lv, F. Niu, Y. Yu, Water droplet impact on superhydrophobic surfaces with microstructures and hierarchical roughness, Sci. China Phys. Mech. Astron. 57 (2014) 1376–1381.
[22] H. Wu, Z. Yang, B. Cao, Z. Zhang, K. Zhu, B. Wu, S. Jiang, G. Chai, Wetting and dewetting transitions on submerged superhydrophobic surfaces with hierarchical structures, Langmuir 33 (2017) 407–416.
[23] H. Wu, K. Zhu, B. Wu, J. Lou, Z. Zhang, G. Chai, Influence of structured sidewalls on the wetting states and superhydrophobic stability of surfaces with dual-scale roughness, Appl. Surf. Sci. 382 (2016) 111–120.
[24] R. Hensel, A. Finn, R. Helbig, S. Killge, H.-G. Braun, C. Werner, In situ experiments to reveal the role of surface feature sidewalls in the Cassie-Wenzel transition, Langmuir 30 (2014) 15162–15170.
[25] Y. Su, B. Ji, K. Zhang, H. Gao, Y. Huang, K. Hwang, Nano to micro structural hierarchy is crucial for stable superhydrophobic and water-repellent surfaces, Langmuir 26 (2010) 4984–4989.
[26] Y. Liu, J. Ma, T. Wu, X. Wang, G. Huang, Y. Liu, H. Qiu, Y. Li, W. Wang, J. Gao, Cost-effective reduced graphene oxide-coated polyurethane sponge as a highly efficient and reusable oil-absorbent, ACS Appl. Mater. Interf. 5 (2013) 10018–10026.
[27] A. Keshavarz, H. Zilouei, A. Abdolmaleki, A. Asadinezhad, Enhancing oil removal from water by immobilizing multi-wall carbon nanotubes on the surface of polyurethane foam, J. Environ. Manage. 157 (2015) 279–286.
[28] M. Huang, Y. Si, X. Tang, Z. Zhu, B. Ding, L. Liu, G. Zheng, W. Luo, J. Yu, Gravity driven separation of emulsified oil-water mixtures utilizing in situ polymerized superhydrophobic and superoleophilic nanofibrous membranes, J. Mater. Chem. A 1 (2013) 14071–14074.
[29] X. Tang, Y. Si, J. Ge, B. Ding, L. Liu, G. Zheng, W. Luo, J. Yu, In situ polymerized superhydrophobic and superoleophilic nanofibrous membranes for gravity driven oil-water separation, Nanoscale 5 (2013) 11657–11664.
[30] P.C. Chen, Z.K. Xu, Mineral-coated polymer membranes with superhydrophilicity and underwater superoleophobicity for effective oil/water separation, Sci. Rep. 3 (2013) 2776.
[31] B. Van Der Bruggen, C. Vandecasteele, T. Van Gestel, W. Doyen, R. Leysen, A review of pressure-driven membrane processes in wastewater treatment and drinking water production, Environ. Prog. 22 (2003) 46–56.
[32] Q. Zheng, Y. Yu, Z. Zhao, Effects of hydraulic pressure on the stability and transition of wetting modes of superhydrophobic surfaces, Langmuir 21 (2005) 12207–12212.
[33] Z. Xue, S. Wang, L. Lin, L. Chen, M. Liu, L. Feng, L. Jiang, A novel superhydrophilic and underwater superoleophobic hydrogel-coated mesh for oil/water separation, Adv. Mater. 23 (2011) 4270–4273.
[34] W. Zhang, Z. Shi, F. Zhang, X. Liu, J. Jin, L. Jiang, Superhydrophobic and superoleophilic PVDF membranes for effective separation of water-in-oil emulsions with high flux, Adv. Mater. 25 (2013) 2071–2076.
[35] G. Kwon, A.K. Kota, Y. Li, A. Sohani, J.M. Mabry, A. Tuteja, On-demand separation of oil-water mixtures, Adv. Mater. 24 (2012) 3666–3671.
[36] A.K. Kota, G. Kwon, W. Choi, J.M. Mabry, A. Tuteja, Hygro-responsive membranes for effective oil-water separation, Nat. Commun. 3 (2012) 1025.
[37] D.G. Venkateshan, M.M. Amrei, A.A. Hemeda, Z. Cullingsworth, J. Corbett, H. Vahedi Tafreshi, Failure pressures and drag reduction benefits of superhydrophobic wire screens, Colloid Surf. A-Physicochem. Eng. Asp. 511 (2016) 247–254.
[38] D.G. Venkateshan, H. Vahedi Tafreshi, Modelling droplet sliding angle on hydrophobic wire screens, Colloids Surf., A 538 (2018) 310–319.
[39] Y. Lu, S. Sathasivam, J. Song, C.R. Crick, C.J. Carmalt, I.P. Parkin, Robust self-cleaning surfaces that function when exposed to either air or oil, Science 347 (2015) 1132–1135.
[40] Z. Jia, W. Lei, H. Yang, G. Wang, Dynamic wetting behavior of vibrated droplets on a micropillared surface, Adv. Mater. Sci. Eng. 2016 (2016) 8409683.
[41] Y. Liu, M. Andrew, J. Li, J.M. Yeomans, Z. Wang, Symmetry breaking in drop bouncing on curved surfaces, Nat. Commun. 6 (2015) 10034.
[42] X. Chen, R. Ma, J. Li, C. Hao, W. Guo, B.L. Luk, S. Li, S. Yao, Z. Wang, Evaporation of droplets on superhydrophobic surfaces: surface roughness and small droplet size effects, Phys. Rev. Lett. 109 (2012) 116101.
[43] W. Choi, A. Tuteja, J.M. Mabry, R.E. Cohen, G.H. McKinley, A modified Cassie-Baxter relationship to explain contact angle hysteresis and anisotropy on non-wetting textured surfaces, J. Colloid Interf. Sci. 339 (2009) 208–216.
[44] D. Tian, X. Zhang, Y. Tian, Y. Wu, X. Wang, J. Zhai, L. Jiang, Photo-induced water-oil separation based on switchable superhydrophobicity-superhydrophilicity and underwater superoleophobicity of the aligned ZnO nanorod array-coated mesh films, J. Mater. Chem. 22 (2012) 19652–19657.
[45] D. Tian, X. Zhang, X. Wang, J. Zhai, L. Jiang, Micro/nanoscale hierarchical structured ZnO mesh film for separation of water and oil, Phys. Chem. Chem. Phys. 13 (2011) 14606–14610.
[46] H. Wu, K. Zhu, B. Cao, Z. Zhang, B. Wu, L. Liang, G. Chai, A. Liu, Smart design of wettability-patterned gradient on substrate-independent coated surfaces to control unidirectional spreading of droplet, Soft Matter 13 (2017) 2995–3002.
[47] Y. Jin, Q. Ke, P. Jiang, Y. Zhu, F. Cheng, Y. Zhang, Highly efficient oil/water separation and excellent self-cleaning surfaces based on 1-triacontanol-polymerized octadecylsiloxane coatings, Appl. Surf. Sci. 351 (2015) 358–366.